2013

Extracting Tidal Variability of Sea Ice Concentration from AMSR-E Passive Microwave Single-Swath Data: A Case Study of the Ross Sea

Stefanie Mack

Laurie Padman

John M. Klinck
Old Dominion University, jklinck@odu.edu

Original Publication Citation

Mack, S., Padman, L., & Klinck, J. (2013). Extracting tidal variability of sea ice concentration from AMSR-E passive microwave single-swath data: A case study of the Ross Sea. *Geophysical Research Letters, 40*(3), 547-552. doi: 10.1002/grl.50128

Extracting tidal variability of sea ice concentration from AMSR-E passive microwave single-swath data: a case study of the Ross Sea

Stefanie Mack,[1] Laurie Padman,[2] and John Klinck[1]

Received 6 November 2012; revised 21 December 2012; accepted 27 December 2012; published 14 February 2013.

[1] The periodic divergence of stress applied by ocean tidal currents to sea ice affects the time-averaged ice concentration (C_{ice}) and heat and freshwater fluxes at the ocean surface. We demonstrate that, at sufficiently high latitudes, tidal variability in C_{ice} can be extracted from single-swath data from the Advanced Microwave Scanning Radiometer–EOS (AMSR-E) satellite passive microwave sensor, although time intervals between swaths are irregular. For the northwest Ross Sea where tidal currents are large, tidal divergence is the dominant cause of C_{ice} variability in winter, with a range of ±0.2 about a mean of ~0.8. Daily-averaged C_{ice} values vary from >0.9 at neap tides to ~0.7 at spring tides. Variability at the fundamental tidal periods is about half that expected from an inverse barotropic tide model for the Ross Sea, suggesting that the measured tidal signal in C_{ice} may be used to diagnose sea ice mechanical properties and ice/ocean coupling. **Citation:** Mack, S., L. Padman, and J. Klinck (2013), Extracting tidal variability of sea ice concentration from AMSR-E passive microwave single-swath data: a case study of the Ross Sea, *Geophys. Res. Lett.*, *40*, 547–552, doi:10.1002/grl.50128.

1. Introduction

[2] Sea ice motion is forced by the atmosphere and the ocean through drag stresses at the upper and lower boundaries, respectively, modified by internal ice stresses and the presence of solid boundaries including coasts and ice-shelf fronts. Velocities of ice-mounted, satellite-tracked drifters show strong tidal signals in some regions [see, e.g., *Heil et al*., 2008]. At sufficiently low ice concentration (C_{ice}), the ice moves in "free drift" (i.e., internal ice stresses can be ignored), where the ice velocity is very close to the underlying ocean velocity [*Padman and Kottmeier*, 2000]. Therefore, if there is a periodic lateral divergence of surface tidal currents, sea-ice motion will also be periodically divergent. In situ observations confirm this "ice accordion" behavior of sea ice [e.g., *Nansen*, 1898; *Geiger and Ackley*, 1998; *Eisen and Kottmeier*, 2000; *Heil et al*., 2008]. The ice accordion can also be seen in RADARSAT wide-swath synthetic aperture radar data at high latitudes [*Kwok et al*., 2003].

[3] Although the tide-forced ice divergence is essentially periodic, numerical models indicate that this process has a net effect on time-averaged sea ice properties including C_{ice} and ice thickness h_{ice} [see, e.g., *Kowalik and Proshutinsky*, 1994]. *Koentopp et al*. [2005] studied the effect on mean sea ice characteristics of adding tides to an atmospherically forced model of the Weddell Sea, where strong tidal motion of sea ice occurs over the continental shelf and upper continental slope [*Geiger and Ackley*, 1998; *Heil et al*., 2008]. Oscillatory sea ice divergence ($\nabla \cdot \mathbf{u}_{ice}$) reduced the modeled, time-averaged value of $C_{ice}(x,y)$ in some regions by up to ~20%, changed mean ice thickness $h_{ice}(x,y)$ by up to ~0.5 m, and led to higher net annual ice growth. Coupling between tidal processes and the mean motion of the sea ice driven by the wind stress and oceanic flow led to modeled tidal effects being distributed well beyond the regions of strong tidal currents.

[4] Given this modeled role of tides on mean sea ice characteristics, we seek an observational method for mapping tide-forced sea ice divergence. *Padman and Kottmeier* [2000] proposed that strong tidal divergence in specific regions, notably along the continental shelf break, might be visible as locally low values of C_{ice} derived from daily-averaged SSM/I passive microwave satellite data. However, the fundamental periodicities of tides (~1/2 and ~1 day) are not resolved by daily-averaged maps, and other processes may affect time-averaged values of C_{ice} along the shelf break. Here, we report a novel method in which we use individual swaths of AMSR-E passive microwave satellite data to develop time series of C_{ice} at high temporal resolution (several times per day) to allow detection of tidal variations of C_{ice}. For this study, we focus on the Ross Sea, Antarctica, which has an extensive winter sea ice pack (Figure 1) and large, spatially variable, tidal currents [*Erofeeva et al*., 2005; *Padman et al*., 2009].

2. Data and Methods

[5] We use Level 2 swath data that were acquired with the AMSR-E passive microwave sensor on the Aqua satellite [*Parkinson*, 2003]. These data are owned and distributed by the Japanese Aerospace Exploration Agency (JAXA) as part of the EOS. Level 2 swath data include values of C_{ice} derived with the modified Bootstrap sea ice concentration algorithm [*Comiso*, 2009], provided at a spacing of ~10 km across swaths that are ~1450 km wide [*JAXA*, 2006].

[6] Aqua is in sun-synchronous orbit and passes over the equator at ~13:30 local solar time [*JAXA*, 2006]. Locations closer to the poles are more frequently sampled by overlapping swaths. At 72° latitude, three to four swaths sample

All Supporting Information may be found in the online version of this article.

[1]Center for Coastal Physical Oceanography, Norfolk, Virginia, USA.
[2]Earth & Space Research, Corvallis, Oregon, USA.

Corresponding author: Corresponding author: S. Mack, Center for Coastal Physical Oceanography, 4111 Monarch Way, 3rd Floor, Norfolk, VA 23529, USA. (mack@ccpo.odu.edu)

0094-8276/13/10.1002/grl.50128

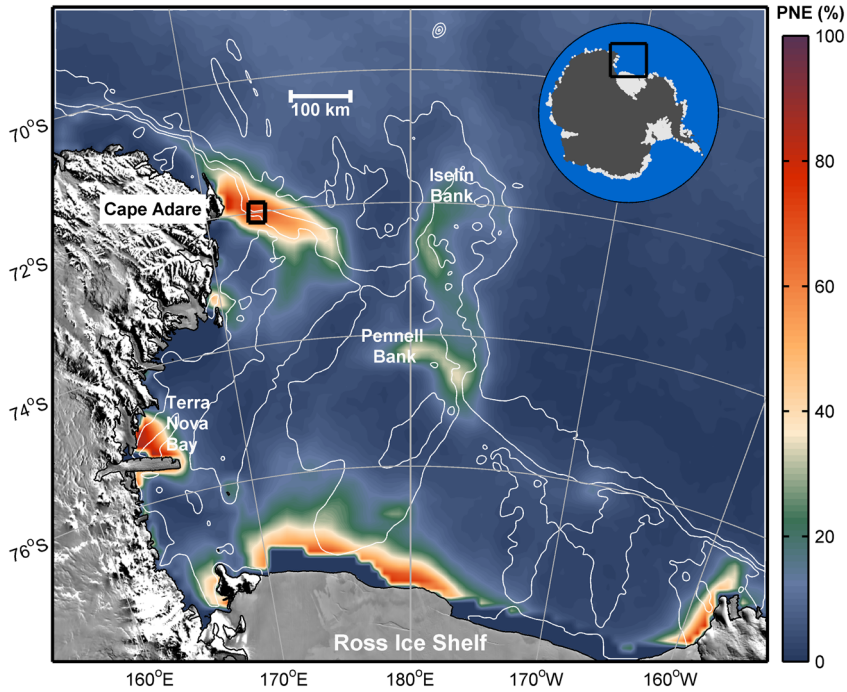

Figure 1. Probability of nonexceedance of sea ice concentration (C_{ice}) in the Ross Sea for a threshold of C_{ice} = 0.95 for all AMSR-E daily-averaged data for April–November inclusive, years 2002–2009. Data were processed with the "NASA Team 2" algorithm [*Markus and Cavalieri*, 2009]. High values imply frequent occurrences of partial open water (leads or polynyas). White lines are 500, 1000, and 2000 m isobaths. The test site is indicated as a black box just to the east of Cape Adare, northwest Ross Sea.

a specific location per day; however, the time separation of consecutive passes is not regular (Figure 2).

[7] To determine whether tidal signals can be extracted from these irregularly sampled data, we first analyzed AMSR-E C_{ice} estimates from individual passes over a test site in the northwest Ross Sea continental slope where we expect the tidal signal in C_{ice} to be large [*Erofeeva et al.*, 2005; *Padman et al.*, 2009]. We extracted C_{ice} values from each satellite swath sampling a box of size 25 × 25 km centered at 72°S, 172.5°E (see Figure 1 for location). The box size is a compromise between the potentially small scales of variability of tidal divergence (set mostly by topography; see *Padman and Kottmeier*, 2000) and the need for sufficient spatial averaging of individual C_{ice} estimates from the swath data. The median number of C_{ice} estimates per box average for each swath is 6 to 8. The time difference of several seconds for individual swath data points over this small area was ignored in assigning a time t to each swath estimate of $C_{ice}(t)$.

[8] We limited further analysis to the "winter" period April–November inclusive, when C_{ice} generally stayed between 0.5 and 1.0 (Figure 3a). The time series of spatially averaged $C_{ice}(t)$ values from each swath was interpolated to a regular 2-h time step using cubic splines. The resulting time series, denoted $C'_{ice}(t)$, was analyzed with the Matlab toolbox, T_Tide [*Pawlowicz et al.*, 2002], to determine amplitude and phase coefficients for major tidal constituents. This package is based on the *Foreman* [1977] analysis code that extracts a best tidal fit using all tidal constituents that can be formally resolved with a given record length. Tide heights and currents in the northwest Ross Sea are dominated by diurnal tidal constituents O_1 (period ~25.82 h) and K_1 (~23.96 h), whereas semidiurnal constituents are negligible [see *Erofeeva et al.*, 2005; *Whitworth and Orsi*, 2006; see Table 1]. The tidal amplitude coefficients for C_{ice} (Table 1) generally show a similar pattern. However, the largest-amplitude tidal signal in C_{ice} is the long-period tide MF with period ~328 h (~13.66 days); this periodicity is the modulation period (spring/neap cycle) of the O_1 and K_1 fundamental tidal constituents.

[9] We tested our analysis procedure by generating a synthetic tidal signal as the sum of two sine waves representing O_1 and K_1 with the same amplitudes given in column 5 of Table 1, then sampling this signal at the satellite pass times, interpolating as described above, and performing the tidal analysis with T_Tide. The analysis method returned the correct primary frequencies and no significant spurious signals; however, amplitudes for O_1 and K_1 were each reduced by ~30% relative to their prescribed values; compare columns 5 and 6 of Table 1. We attribute this reduction to the large daily

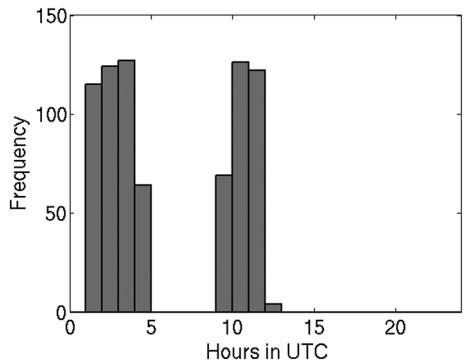

Figure 2. Frequency of swath passes over the study location over the course of 1 year. The irregular satellite sampling leaves 12 consecutive hours unsampled.

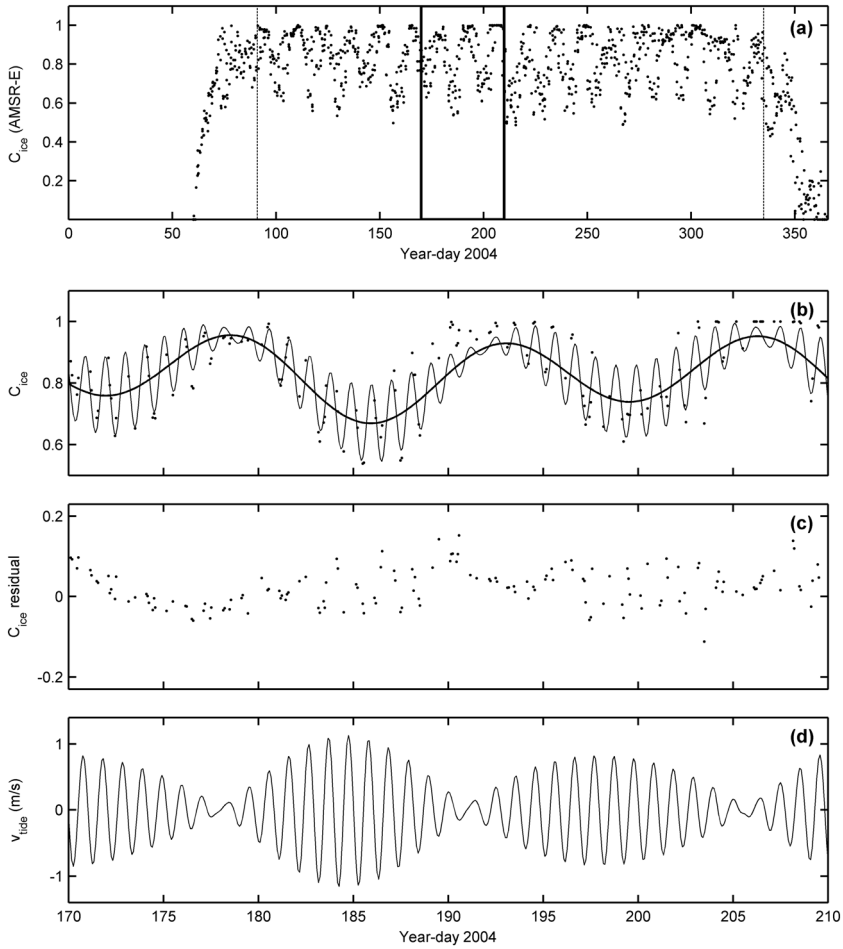

Figure 3. Sea ice concentration (C_{ice}) and tidal properties for year 2004 for a site in the northwest Ross Sea east of Cape Adare; see Figure 1 for location. (a) Measured values of $C_{ice}(t)$ for each swath, spatially averaged in a 25 × 25 km box. Vertical dashed lines show period for which tidal analysis was performed with T_Tide (see Table 1). Vertical solid lines demark time interval shown in (b)–(d). (b) Values of C_{ice} for each swath (dots), tidal contribution based on T_Tide fit (continuous light line), and tidal contribution associated with long-period tides (continuous heavy line). (c) Residual C_{ice} anomaly after removal of tidal fit. (d) Cross-slope velocity v (m s^{-1}) evaluated with the RossTIM barotropic tidal inverse model [*Erofeeva et al.*, 2005].

gap (~12 h; see Figure 2) in data, which is interpolated across by the cubic splines.

[10] Note that the amplitude of the long-period MF constituent from the tidal analysis of the synthetic time series (~0.009) is small compared with the value of ~0.096 from our analysis of AMSR-E swath data. This observation indicates that the large MF signal in measured C_{ice} is not an artifact of the analysis procedure but represents some true geophysical variability over spring/neap cycles.

[11] Sea-ice concentration products are routinely distributed as daily values that are derived as simple arithmetic means of all instantaneous C_{ice} measurements in a specific grid cell during 1 day. (For AMSR-E, a 12.5 × 12.5 km polar stereographic grid is used.) The irregular time sampling by swaths (Figure 2) suggests that this approach to constructing daily averages may alias diurnal tidal constituents, whose periods differ slightly from 1.0 solar day, to longer periods. To test whether this aliasing occurs in practice, we calculated daily arithmetic mean values of our synthetic signal sampled at the satellite pass times. This analysis shows a signal near 14 days (Figure S1 in the Supporting Information). Although

Table 1. Amplitudes of Major Tidal Harmonics at the Test Site Centered on 72°S, 172.5°E in the Northwest Ross Sea (See Figure 1 for Location)[a]

Constituent	Period (h)	Elevation (m)	Cross-Slope Current (cm s^{-1})	C_{ice}	C_{ice} Synthetic
Long period					
MF	327.86	0.03	0.02	0.096	0.009
Diurnal					
O1	25.82	0.27	48.7	0.070	0.050
K1	23.96	0.22	30.6	0.046	0.033
P1	24.00	0.09	9.9	0.006	0.007
Semidiurnal					
M2	12.42	0.09	0.7	NS	NS
S2	12.00	0.06	0.9	NS	NS

[a]Column 2 lists component periods in hours. Columns 3 and 4 give amplitudes for sea surface elevation and barotropic cross-slope tidal current, respectively, from the RossTIM barotropic tidal inverse model. Column 5 lists amplitudes of variability in C_{ice} from the present study. Column 6 is the tidal analysis of a synthetic signal created using O_1 and K_1 signals only, processed, and analyzed as described in Section 2. NS, nonsignificant.

we expect a ~14-day cycle in tidal range due to the superposition of O_1 and K_1, the daily-averaged values in the synthetic signal are close to zero regardless of time within the spring/neap cycle.

[12] We also applied the same analysis method to a simpler synthetic signal composed of a single sine wave with period ~24.89 h equal to the average of O_1 and K_1 periods. In this case, the daily averages show a period of 27.4 days with amplitude ~60% of the original sine wave, which is entirely a product of the irregular sampling scheme. The ~14- and ~27-day periods from aliased fundamental tides may be misinterpreted as weather-band variability in C_{ice}. These results can be generalized to any sun-synchronous satellite observing phenomena with near-daily periodicity.

3. Results and Discussion

[13] The time series of area-averaged, single-swath values of $C_{ice}(t)$ for the 25 × 25 km box centered on 72°S, 172.5°E shows values ranging from ~0.5 to 1.0 with a mean of 0.84 for April–November inclusive, 2004 (Figure 3a). The T_Tide analysis applied to the interpolated time series $C'_{ice}(t)$ (Table 1) shows significant O_1 and K_1 signals with C_{ice} amplitude coefficients of 0.070 ± 0.007 and 0.046 ± 0.007, respectively, and a large MF (period ~13.7 days) tide with amplitude ~0.096. We estimated the errors for O_1 and K_1 amplitudes by a Monte Carlo approach, assuming that the standard deviation of measurement uncertainty for $C_{ice}(t)$ is ~0.1 [*Comiso*, 2009; see Supporting Information for further information].

[14] The MF signal represents the observed reduction from high daily-averaged ice cover ($C_{ice} > 0.9$) at neap tides to typical values of ~0.7 at spring tides (Figure 3b). The large MF signal is not the result of aliasing of the O_1+K_1 signal by irregular temporal sampling; compare columns 5 and 6 of Table 1.

[15] The amplitude of the residual signal in C_{ice}, after removing the fitted tidal variability including long-period tides, is smaller than the tidal component (compare Figures 3c and 3b). That is, tides explain most variability of C_{ice} at this location during winter.

[16] To place the tidal signals in C_{ice} in the context of ocean tidal state, we use the Ross Sea Tidal Inverse Model (RossTIM) [*Erofeeva et al*., 2005] to estimate the depth-averaged cross-slope tidal velocity (Figure 3d). The RossTIM model assimilates velocities from moorings and ship-based acoustic Doppler current profiles from cruises near the northwest Ross Sea shelf break and so is the best available model for predictions of barotropic tidal currents in this region. The spring/neap cycle of $C'_{ice}(t)$ (Figure 3b) is approximately out of phase with the spring/neap cycle in modeled cross-slope ocean tidal velocity; the lowest daily-averaged values of C_{ice} occur about 1 day after maximum spring tidal currents.

[17] We expect that the major effect of ocean tides on C_{ice} at the fundamental diurnal tidal periods is caused by tidal divergence [*Padman and Kottmeier*, 2000]. Tides in the northwest Ross Sea also cause warmer offshore water to flood onto the outer continental shelf [*Padman et al*., 2009]; however, we do not expect these warmer waters to significantly change ice concentration by melting because individual ice floes are advected quite rapidly through the region where tidal advective effects are significant (see *Comiso et al*., 2011, for maps of measured ice velocity). Thus, for the remainder of this article, we focus on changes in C_{ice} associated with predicted periodically divergent tidal stresses.

[18] By applying the above analysis of AMSR-E swath C_{ice} data to 25 × 25 km boxes covering the entire Ross Sea, we have developed maps of amplitude and phase coefficients for O_1 and K_1 constituents (Figure 4). Boxes with a signal-to-noise ratio (SNR) < 3, based on T_Tide output, have been hidden. Amplitudes for both O_1 and K_1 sometimes exceed 0.05 over the continental slope in the northwest Ross Sea, and significant values (SNR > 3) are found along much of the continental slope and over Iselin Bank (see Figure 1 for location). Phase maps (Figure 4, top) show westward propagation of C_{ice} anomalies along the continental slope, consistent with diurnal tidal currents being primarily associated with small-scale topographic vorticity waves trapped to the slope [cf. *Padman and Kottmeier*, 2000; *Erofeeva et al*., 2005].

[19] We used the RossTIM model and the same averaging scale (25 × 25 km) applied to swath estimates of C_{ice} to estimate the horizontal divergence of ocean tidal currents ($\nabla_h \cdot \mathbf{u}_{ocean}$) for each of O_1 and K_1. The standard deviation of lateral divergence, $\sigma(\nabla_h \cdot \mathbf{u}_{ocean})$, can then be converted to the amplitude coefficient (A) of the open-water fraction for a specific tidal constituent, assuming free drift of sea ice, by

$$A = \sigma(\nabla_h \cdot \mathbf{u}_{ocean}) T_{tide} / 2^{1/2} \pi, \quad (1)$$

where T_{tide} is the period of the constituent. Peak values of $\sigma(\nabla_h \cdot \mathbf{u}_{ocean})$ are ~10^{-5} s^{-1}, implying $A \approx 0.2$ for a single constituent of the diurnal tide. However, the values of A based on RossTIM are typically about twice as large as the values derived from our analyses of AMSR-E swath data (compare Figure 4, middle and bottom). The RossTIM model does not include the long-period MF tidal constituent; however, analyses of predicted values of $\sigma(\nabla_h \cdot \mathbf{u}_{ocean})$ for MF in other tide models suggest that the divergence for this constituent is much too small to explain the observed MF signal in $C_{ice}(t)$, although T_{tide} is large (~14 days).

[20] Because RossTIM is based on assimilation of tidal current data [*Erofeeva et al*., 2005], we expect that it is a reasonable representation of lateral divergence of barotropic tidal ocean currents at the fundamental tidal periods of ~1 and ~0.5 day. Thus, we interpret the discrepancies between measured and modeled values of A for O_1, K_1, and MF as indicating weaknesses in the free-drift assumption used to equate $\nabla \cdot \mathbf{u}_{ice}$ to $\nabla_h \cdot \mathbf{u}_{ocean}$ and/or the presence of baroclinic tidal signals that reduce the near-surface tidal divergence relative to the barotropic (depth-averaged) value. Identifying these processes is beyond the scope of the present study; however, the existence of these discrepancies suggests that tidal analyses of C_{ice} measurements from AMSR-E swath data may be used to diagnose sea ice mechanical properties and ice/ocean coupling.

4. Conclusions

[21] At sufficiently high latitudes, the tidal contribution to sea-ice concentration variability can be evaluated from analyses of individual swaths of AMSR-E satellite passive microwave data. For a typical latitude of ice-covered polar seas, ~72°, we obtain approximately three to four passes per day, which is sufficient to quantify diurnal tidal variability. For higher-latitude locations such as the southern Ross and Weddell seas, and the Arctic Ocean, swath data are acquired more frequently. However, many of these locations are

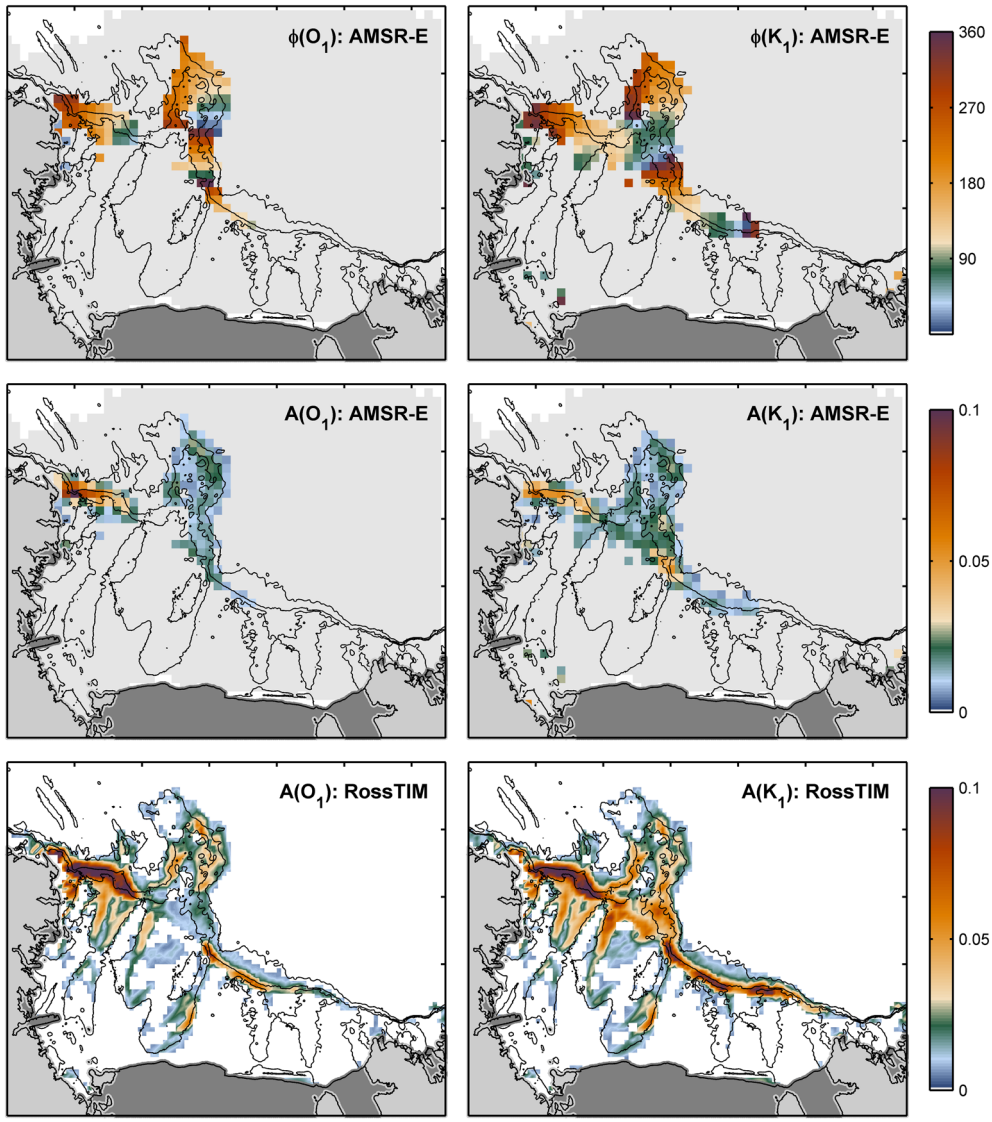

Figure 4. (left, top and middle) Phase and amplitude of C_{ice} variability for the O_1 tidal constituent from T_Tide analysis of AMSR-E swath data in 25 × 25 km boxes. Boxes with a SNR < 3 (determined by T_Tide) are not plotted. Amplitude has been scaled by 1.2 to account for signal reduction associated with interpolation of the irregular time series of swath data (see Table 1). (left, bottom) Amplitude of C_{ice} variability based on the barotropic inverse tide model RossTIM, using 25 × 25 km boxes to calculate horizontal divergence of O_1 tidal currents ($\nabla_h \cdot \mathbf{u}_{ocean}$), and assuming free drift of sea-ice. Values < 0.005 are not plotted. (right) Same as left, but for K_1 tidal constituent. In all panels, black contours are 500, 1000, and 2000 m isobaths.

dominated by semidiurnal (period ~1/2 day) rather than diurnal tides, thus requiring more frequent passes to adequately sample the fundamental tides.

[22] For our study region in the northwest Ross Sea, sea ice response to ocean tidal currents causes C_{ice} to vary in winter (April–November inclusive) by up to ±0.2 around a mean value of ~0.8. Variability of this magnitude could have a significant impact on the average heat exchange between the atmosphere and ocean and net sea ice production, much like a small polynya.

[23] We hypothesize that the time-averaged value of C_{ice} over the northwest Ross Sea continental slope is itself lower than it would be in the absence of tides. Our conceptual model is that, in winter, sea ice is advected from the south at ~0.1 m s^{-1} [*Comiso et al.*, 2011] as almost solid ice pack (Figure 1). As the pack ice transits the shelf break and continental slope, it is relatively unaffected if it crosses during neap tides but is periodically forced open by tidal divergence during spring tides (Figure 3). This intermittent creation of open water (i.e., leads) in an ice pack that would otherwise have $C_{ice} \approx 1$ implies dynamic thickening of ice floes by rafting and by ridge building at floe margins as new ice formed in the transient leads is compressed in each subsequent convergent phase.

[24] Ice resistance to deformation explains the reduction of O_1 and K_1 tidal components of $C_{ice}(t)$ relative to the values estimated from a barotropic inverse tidal model and the free-drift approximation. The strong spring/neap cycle of C_{ice} (Figure 3b) is consistent with coupling between mean advection and the spatially limited region of strong tidal currents. It is also possible that baroclinicity of the tidal currents leads to a reduction in surface values of $\nabla_h \cdot \mathbf{u}_{ocean}$

relative to the modeled barotropic (depth-averaged) values, but we have seen no evidence for significant baroclinic tides in the weakly stratified Ross Sea. We are exploring these hypotheses using a 3-D ocean model coupled to a dynamic/thermodynamic sea ice model of this region.

[25] We have also demonstrated that, because of the irregular time sampling by satellite swaths, simple daily averages of C_{ice} (as typically provided to users) can alias diurnal tides to lower frequencies (~1 and ~2 cycles per month), where the signal may be confused with wind-forced and other low-frequency variability in C_{ice}. An improved approach to daily averaging is to fit tidal harmonics to estimates of C_{ice} at times of individual swaths and then calculate the average of the fitted time series.

[26] The AMSR-E single-swath data set and the methodology described above are best suited to high-latitude regions where ocean tidal divergence is strong and other causes of C_{ice} variability at high frequencies are relatively weak. Such regions include the ice-shelf fronts and shelf breaks of the Ross and Weddell seas in Antarctica and the eastern Arctic Ocean. Further analyses of the AMSR-E ice concentration record may provide valuable information not only on the sea ice cover but also on the state of the underlying ocean and our ability to model it.

[27] **Acknowledgments.** We thank Chet Grosch for his invaluable insights into time series and data analysis techniques, Mike Dinniman and Pierre St. Laurent for their suggestions and support, Susan Howard for computational assistance, and Ron Kwok and an anonymous reviewer for their comments on the original submitted manuscript. This study was funded by NASA grant NNX08AN676 and National Science Foundation Major Research Instrumentation award 0722644, which supported the purchase of ESR's cluster computer. This is ESR contribution 147.

References

Comiso, J. C. (2009), Enhanced Sea Ice Concentrations and Ice Extents from AMSR-E Data, *J. Remote Sensing Soc. Japan*, *29*(1), 199–215.

Comiso, J. C., R. Kwok, S. Martin, and A. L. Gordon (2011), Variability and trends in sea ice extent and ice production in the Ross Sea, *J. Geophys. Res.*, *116*, C04021.

Eisen, O., and C. Kottmeier (2000), On the importance of leads in sea ice to the energy balance and ice formation in the Weddell Sea, *J. Geophys. Res. 105*(C6), 14045–14060.

Erofeeva, S. Y., G. D. Egbert, and L. Padman (2005), Assimilation of ship-mounted ADCP data for barotropic tides: Application to the Ross Sea, *J. Atmos. Oceanic Technol.*, *22*, 721–734.

Foreman, M. G. G. (1977; revised 2004), Manual for tidal heights analysis and prediction, *Pacific Marine Science Report*, 77-10, Institute of Ocean Sciences, Patricia Bay, 58 pp.

Geiger, C. A., and S. F. Ackley (1998), Large-scale sea ice drift and deformation: Comparison between models and observations in the western Weddell Sea during 1992, *J. Geophys. Res.*, *103*(C10), 21,893–21,914.

Heil, P., J. K. Hutchings, A. P. Worby, M. Johansson, J. Launiainen, C. Haas, and W. D. Hibler III (2008), Tidal forcing on sea-ice drift and deformation in the western Weddell Sea in early austral summer, 2004, *Deep Sea Res. Part II*, *55*, 943–962.

JAXA (Japan Aerospace Exploration Agency) (2006), AMSR-E Data Users Handbook, 115 pp, March 2006 (http://www.eorc.jaxa.jp/en/hatoyama/amsr-e/amsr-e_handbook_e.pdf).

Koentopp, M., O. Eisen, Ch. Kottmeier, L. Padman, and P. Lemke (2005), Influence of tides on sea ice in the Weddell Sea: Investigations with a high-resolution dynamic-thermodynamic sea ice model, *J. Geophys. Res.*, *110*, C02014, doi:10.1029/2004JC002405.

Kowalik, Z., and A. Y. Proshutinsky (1994), The Arctic Ocean Tides, in The Polar Oceans and Their Role in Shaping the Global Environment, Geophysical Monograph 85, edited by O. M. Johannessen, R. D. Muench, and J. E. Overland, pp. 137–158, AGU, Washington, D. C.

Kwok, R., G. F. Cunningham, and W. D. Hibler III (2003), Sub-daily sea ice motion and deformation from RADARSAT observations, *Geophys. Res. Lett.*, *30*(23), doi:10.1029/2003GL018723.

Markus, T., and D. J. Cavalieri (2009), The AMSR-E NT2 sea ice concentration algorithm: Its basis and implementation, *J. Remote Sensing Soc. Japan*, *29*(1), 216–225.

Nansen, F. (1898), *Farthest North*, George Newnes, Ltd., London.

Padman, L., S. L. Howard, A. Orsi, and R. Muench (2009), Tides of the northwestern Ross Sea and their impact on dense outflows of Antarctic Bottom Water, *Deep Sea Res. Part II*, *56*, 818–834, doi: 10.1016/j.dsr2.2008.10.026.

Padman, L., and C. Kottmeier (2000), High-frequency ice motion and divergence in the Weddell Sea, *J. Geophys. Res.*, *105*(C2), 3379–3400.

Parkinson, C. L. (2003), Aqua: An Earth-Observing Satellite Mission to Examine Water and Other Climate Variables, *IEEE Trans. Geosci. Remote Sens.*, *41*(2), 173–183.

Pawlowicz, R., R. Beardsley, and S. Lentz (2002), Classical tidal harmonic analysis including error estimates in MATLAB using T_TIDE, *Comput. Geosci.*, *28*, 929–937.

Whitworth III, T., and A. Orsi (2006), Antarctic Bottom Water production and export by tides in the Ross Sea, *Geophys. Res. Lett.*, *33*, L12609.